ROYAL SOCIETY
OF CHEMISTRY

PAPER

Check for updates

Synthesis of green-based carbon-doped nanosilica for enhanced mechanical properties of coconut oil-based rigid polyurethane foam

Carlo Kurt F. Osorio,[a] Christine Joy M. Omisol,[a] Dan Michael A. Asequia,[a]
Blessy Joy M. Aguinid,[a] Daisy Jane D. Erjeno,[a] Kassandra Jayza Gift D. Tejas,[a]
Roger G. Dingcong, Jr.,[a] Tomas Ralph B. Tomon,[a] Renzo Miguel R. Hisona,[a]
Andrei E. Etom,[a] Ann Pearl G. Triana,[a] Gerard G. Dumancas,[c,d] Arnold C. Alguno,[a,e]
Joshua B. Zoleta,[e] Roberto M. Malaluan[a,b] and Arnold A. Lubguban ★[a,b]

High-strength, bio-based rigid polyurethane foam (RPUF) was synthesized using coconut oil-based polyol reinforced with green silica nanoparticles (SNP) derived from rice husk ash (RHA). The SNPs were carbon-doped using κ-carrageenan to enhance their functional properties. Comprehensive characterization of the synthesized SNP and SNP-enhanced RPUF was conducted using Fourier-transform infrared spectroscopy (FTIR), X-ray diffraction (XRD), dynamic light scattering (DLS), and scanning electron microscopy with energy dispersive X-ray spectroscopy (SEM-EDX). X-ray photoelectron spectroscopy (XPS) confirmed successful κ-carrageenan-mediated carbon doping, improving SNP reactivity. The incorporation of SNP (up to 0.3% by mass) significantly enhanced the compressive strength of RPUF by 92.42%, attributed to hydrogen bonding and induced crosslinking interactions between the SNP and amine groups in the bio-polyol, as evidenced by FTIR, SEM, and pycnometric analyses. Thermogravimetric analysis (TGA) demonstrated that SNP integration improved the thermal stability of RPUF without compromising its thermal conductivity, meeting industrial standards. This study highlights the potential of sustainably derived nanomaterials to improve the mechanical and thermal properties of bio-based composites. Furthermore, the SNP-reinforced RPUF offers promising applications in environmentally friendly materials for thermal insulation, structural components, and environmental remediation, contributing to the development of high-performance, sustainable materials for various industrial applications.

Introduction

Silica nanoparticles (SNPs) are one of the most widely studied nanomaterials due to their high surface area, porosity, and functionality.[1] These attributes render SNPs indispensable across a broad spectrum of applications, ranging from the biomedical field,[2] such as in bio-sensing and drug transportation, to catalysis support[3] and material fillers.[4,5] The versatility of

[a]*Center for Sustainable Polymers, Mindanao State University – Iligan Institute of Technology, Iligan City 9200, Philippines. E-mail: arnold.lubguban@g.msuiit.edu.ph*
[b]*Department of Chemical Engineering and Technology, Mindanao State University – Iligan Institute of Technology, Iligan City 9200, Philippines*
[c]*Honors College, Henry E. and Shirley T. Frye Hall, Suite 110, North Carolina Agricultural & Technical State University, 1601 East Market Street, Greensboro, NC 27411, USA*
[d]*Department of Chemistry, New Science Building, North Carolina Agricultural & Technical State University, 1601 E. Market Street, Greensboro, NC 27411, USA*
[e]*Department of Materials and Resources Engineering & Technology, Mindanao State University – Iligan Institute of Technology, Iligan City 9200, Philippines*

SNPs has spurred considerable interest in optimizing their synthesis and functionalization to enhance their utility in various advanced applications further.

Recent research has increasingly focused on developing green and environmentally friendly synthesis methods for SNPs. Traditional synthesis techniques, including sol–gel and reverse micro-emulsion processes, while effective, pose significant environmental, safety, and economic challenges. These methods are often associated with high energy demands, toxic chemical use, waste generation, scalability issues, and high production costs.[6] In response to the limitations of traditional synthesis methods, numerous studies have investigated alternative routes that utilize natural resources, such as leaf extracts, bacterial processes, and agricultural waste products, as sustainable and eco-friendly feedstocks.[7] These approaches offer promising paths toward more environmentally responsible and economically viable solutions for nanomaterial production, aligning with the principles of green chemistry and circular economy.

Agriculture wastes, particularly rice husks, have garnered significant attention for SNP production. Rice husks are abundant and often disposed of in ways that harm the environment. Utilizing rice husks for SNP production not only offers a sustainable source of silica but also addresses waste management issues.[8] Various extraction techniques, including thermal, chemical, hydrothermal, and carbonation processes, have been investigated to derive SNPs from rice husks. These methods represent a diverse array of green synthesis methodologies that hold promise for large-scale, environmentally benign SNP production.[9]

The functionalization of nanoparticles is at the forefront of nanomaterials research, enabling the customization of SNPs for a wider array of complex applications. Surface modifications are a common strategy for functionalizing SNPs. This typically involves integrating metals or organic compounds onto the SNP surface using coupling agents such as silane-based compounds.[10] Such modifications can tailor the surface properties of SNPs, enhancing their compatibility and performance in specific applications like drug delivery and cancer therapy.[11]

Another functionalization approach involves the use of capping agents to control the size and surface characteristics of SNPs. Green-based materials, such as plant extracts, have been employed as capping agents to produce smaller, more uniform nanoparticles.[12,13] Additionally, doping nanoparticles, such as carbon-doping (C-doping), significantly enhances the photoelectric and reactivity of SNPs. By altering the crystal formations, C-doping increases the number of reactive sites, improves dispersibility, and enhances chemical interactions.[13] These modifications can substantially boost the mechanical strength, thermal stability, and electrical conductivity of SNPs, making them highly suitable for incorporation into polymer matrices such as polyvinyl alcohol (PVA), polypropylene (PP), polystyrene (PS), and polyurethane (PU).[2]

PU is a versatile polymer extensively used in numerous industrial applications, including thermal insulation, flexible foams, coatings, adhesives, and elastomers. As of 2023, the global production of PU was valued at approximately 89.92 billion USD, with a compound annual growth rate (CAGR) of 14.6%.[14] In Southeast Asia alone, PU production reached 3.32 billion USD in 2021, with an expected CAGR of 5.3%.[15] Despite its widespread use and economic importance, conventional PU synthesis heavily relies on non-renewable fossil fuels, contributing to significant environmental challenges due to the production of non-biodegradable waste.

In light of growing concerns over fossil fuel depletion and environmental sustainability, both research institutions and industry players have been driven to seek more sustainable alternatives. This has led to the development of bio-based foams, which feature sustainable polyols derived from vegetable oils such as castor, soybean, palm, rapeseed, and coconut.[16,17] The global market for bio-foams was valued at 126 million USD in 2023 and is projected to grow at a high CAGR of 22.1%,[18] reflecting the increasing demand for environmentally friendly materials.

The properties of PU foam are highly influenced by the additives incorporated during its synthesis.[19,20] Typical additives include blowing agents, catalysts, surfactants, fillers, and pigments, each playing a crucial role in determining the morphology and properties of the final product.[21,22] Among these, nanoparticles are particularly notable for their ability to enhance the performance of PU foams. Depending on their type and functionality, nanoparticles can facilitate the chemical reactions involved in PU formation or serve as fillers reinforcing the PU matrix.

Several studies have demonstrated the effectiveness of SNPs in improving the properties of PUs. These studies often focus on advanced and functionalized SNPs to achieve significant enhancements in mechanical strength, thermal stability, and other desirable properties.[23–25] However, there is a lack of research focused on utilizing sustainably sourced and functionally enhanced silica nanoparticles—such as carbon-doped SNPs derived from rice husk ash and κ-carrageenan—in the synthesis and enhancement of rigid polyurethane foams (PU) composites.

In this study, we aim to explore the potential of using green-based materials as raw resources for both nanoparticle and polymer synthesis. Specifically, we investigate the synthesis of high-strength rigid PU foam (RPUF) composites using SNPs derived from rice hull ash doped with carbon from κ-carrageenan and functionalized bio-polyol sourced from coconut oil. This approach not only utilizes sustainable raw materials but also aims to enhance the properties of the resulting PU composites.

A comprehensive analysis of the functionalities of both the SNPs and the bio-polyol is conducted, encompassing their chemical, morphological, mechanical, and thermal properties. By integrating green synthesis methodologies and advanced functionalization techniques, this study seeks to elucidate the potential of sustainable materials in polymer engineering applications, paving the way for more eco-friendly and high-performance nanocomposites.

Materials and methods

Materials

Rice husk (RH) was sourced from local rice farms in Iligan City, Philippines, as a silica source, and κ-carrageenan, as a dopant, was acquired from MSU Tawi-Tawi. Hydrochloric acid (HCl), sulfuric acid (H_2SO_4), and sodium hydroxide (NaOH) were procured from Sigma-Aldrich Chemicals (Philippines). The SNP-RPUFs were developed using coconut diethanolamide (p-CDEA) as a bio-polyol and synthesized in the laboratory. Refined, bleached, and deodorized coconut oil was purchased from GranexPort Manufacturing Corporation in Iligan City, Philippines. Reagent-grade Diethanolamine (DEA) and refined glycerol were purchased from Ajax Finechem and Sigma-Aldrich, respectively. Polymeric diphenylmethane-4,4-diisocyanate (pMDI, PAPI 135H, with 31.4 wt% NCO and a functionality of 2.7) was kindly provided by Chemrez Technologies, Inc.

© 2025 The Author(s). Published by the Royal Society of Chemistry

RSC Appl. Polym., 2025, **3**, 1356–1365 | **1357**

(Quezon City, Philippines). The amine catalyst (Polycat® 8), CaO, ZnO, and surfactant (INV 690) were obtained from Evonik Industries (Germany).

Synthesis of p-CDEA

p-CDEA was prepared using the established method by Dingcong et al., 2023.[26] Specifically, coconut oil was first subjected to glycerolysis by reacting refined glycerol using a CaO catalyst in a closed PARR reactor while maintaining the reaction temperature at 220 °C for 2 hours with high-speed stirring at 1500 rpm. 10% DEA was added, with an additional 0.015% ZnO catalyst for the amidation reaction. The reaction was maintained at 140 °C for 4 hours. A dark yellow polyol (Fig. 1A), denoted as p-CDEA, was produced that is mainly composed of diethanolamide, whose actual photograph and chemical structure are illustrated in Fig. 1.

Preparation of SNP

The synthesis of SNP was prepared using improved methods based on related literature.[27,28] Rice husk (RH) was washed thoroughly with water to remove the soluble particles, dust, and other contaminants present, whereby heavy impurities such as sand were also removed. It was then dried in an air oven at about 110 °C for 24 hours. An acid-washing step was used to remove the small quantities of minerals before silica extraction from rice husk ash (RHA). The rice husk sample is submerged, stirred, and heated in 1 M HCl for 1 hour at 60 °C. The RH was subjected to heat treatment to obtain the ash. Samples were burned inside a muffle furnace at 350 °C for 4 hours. The obtained RHA was subsequently reacted with sodium hydroxide and water at a ratio of 1.20 g NaOH per g of RHA. The solution was heated in a covered beaker by stirring constantly, allowed to stand at room temperature, and filtered to produce sodium silicate. 25 mL of 1% κ-carrageenan was added to 75 mL of the produced sodium silicate. H_2SO_4 was added until neutralized. The precipitate silica was washed repeatedly with deionized water and then centrifuged at a speed of 4500 rpm for 15 minutes. The product was aged at 50 °C for 12 hours in the oven, calcined at 700 °C for 2 hours, then crushed to collect the SNP.

Preparation of SNP-RPUF

The synthesis of RPUF with SNP was derived from related literature.[26,29] The B-side components of the RPUF, consisting of p-CDEA, amine catalyst, silicone surfactant, and SNP of

different loadings (0.0%, 0.1%, 0.2%, 0.3%, 0.4%, and 0.5%), were premixed in a paper cup for 60 s using a high-speed mixer at 1000 rpm. The premixture was degassed for 60 s before the A-side (pMDI) was rapidly added with continuous stirring for another 10 to 15 s at 3000 rpm. The amount of pMDI was calculated using eqn (1) at a constant isocyanate index of 110.[30] The reactive mixture was promptly transferred into a rectangular mold (11.4 cm × 11.4 cm × 21.6 cm), where it underwent free-rise foaming driven by CO_2 evolution from the reaction between the water blowing agent and excess pMDI.[31]

The foam was allowed to rise and cure under ambient conditions (25 °C, 1 atm).

The synthesized RPUFs were then cured for 7 days before characterizations were done.

$$m_{pMDI} = ISO \times \frac{(OH_n \times m_p) + (56 \times m_{water})}{W_{NCO}} \quad (1)$$

where, m_{pMDI} is the amount of required pMDI; ISO is the isocyanate index; OH_n is the hydroxyl value; m_{water} is the amount of water added as the blowing agent; W_{NCO} is the pMDI NCO content, and 56 is the conversion factor from mg KOH to mmol OH equivalent.

Characterization of p-CDEA

The synthesized p-CDEA's hydroxyl (OH) number, acid value, and iodine value were characterized using ASTM D4274-16, ASTM D664, and ASTM D5678, respectively. The molecular weight was determined using a Shimadzu Prominence gel permeation chromatography (GPC) system equipped with a refractive index detector and a Shodex GPC column (Shimadzu Corp., Kyoto, Japan) following ASTM D6474.

Characterization of SNP and SNP-RPUF

Fourier Transform Infrared Spectroscopy (FTIR) with Attenuated Total Reflectance (ATR) was used to confirm and study the functional groups present on the SNP and SNP-RPUF samples using a Shimadzu IRTracer-100 with QATR-10 single reflection ATR. The wavenumber range included was 400–4000 cm^{-1} at a resolution of 4 cm^{-1}.

X-ray diffraction (XRD) patterns of the SNP powder were captured using a Cu Kα radiation source (40 kV and 30 mA) within a 3–90° 2θ range, employing 0.02° 2θ/0.60 s on a Shimadzu XRD Maxima 7000 instrument from Japan. The SNP crystal was confirmed by comparing the prominent positions of reported peaks with those in the standard JCPDS database. The average grain sizes D were also calculated using the Scherrer equation: $D = K\lambda/(\beta \cos \theta)$, where K is the Scherrer constant (0.89), λ is the wavelength of the X-ray (1.54 Å), β is the half-peak width, and θ is the diffraction angle.

Dynamic Light Scattering (DLS) analysis of SNP was determined using a Nanotrac Wave II Dynamic Light Scattering (DLS) instrument (Microtrac MRB, York, PA, USA). The instrument employs heterodyne backscatter detection with a 780 nm laser and operates within a size range of 10 nm to 20 μm
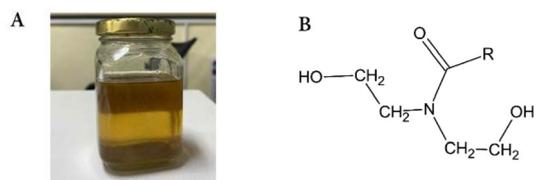

Fig. 1 (A) An actual photograph of p-CDEA polyol and (B) chemical structure of p-CDEA.

coupled with a zeta potential analyzer. One (1) mg ml^{-1} of SNP samples were sonicated for 30 minutes before the samples were analyzed to the equipment.

X-ray photoelectron spectroscopy (XPS) was performed using a JEOL JPS-9200 spectrometer (JEOL Ltd, Japan), which is equipped with a monochromated Al Kα X-ray source running at 100 W in an ultrahigh vacuum environment (approximately 107 Pa).

Closed-cell content was analyzed using an Ultrapyc 5000 Foam gas pycnometer from Anton-Paar in Graz, Austria. The analyses were done using nitrogen gas at 25 °C. The closed cell content (%) was calculated according to ASTM D6266-21, with the apparent densities of the SNP-RPUF foam samples also measured at room temperature following ASTM D1622.

The compressive properties were determined at room temperature using the universal testing machine Shimadzu AGS-XSeries from Kyoto, Japan. The compressive test was performed in accordance with ASTM D1621-04a, using a cross-head speed of 5 mm min^{-1} and cubic samples measuring 50 × 50 × 50 mm. Each sample was compressed up to approximately 50% strain to ensure deformation beyond the yield point and capture post-yield behavior.

The morphological structure of the synthesized SNP and SNP-RPUF samples was observed using a scanning electron microscope (SEM) (JEOL JSM-6510LA). Using the images from SEM, the cell density equation is $N = (nM^2/A)1.5$, where N is the cell density (cells per μm^3), A is the area of the SEM image, M is the magnification factor, and n is the number of cells counted from the SEM images.[32]

Thermogravimetric (TGA) analyses were carried out using a thermogravimetric analyzer (PerkinElmer TGA 4000, Waltham, MA). Samples with an approximate weight of 5 mg were heated from room temperature to 800 °C under a nitrogen atmosphere at a heating rate of 10 °C min^{-1}.

The thermal conductivity of RPUF and SNP-RPUFs was measured through the transient plane source technique (ASTM C518-21) using a heat flow meter (Laser Comp FOX 200 HFM, TA Instruments, USA). The measurements of the factors were made at an average temperature of 25 °C.

Results and discussion

Characterization of p-CDEA

Table 1 summarizes the key properties of the synthesized p-CDEA polyol relevant to rigid polyurethane foam appli-

cations. The hydroxyl value of 361 mg KOH per g exceeds the minimum requirement (~350 mg KOH per g), indicating sufficient functionality for effective crosslinking. Its low acid value (4.3 mg KOH per g) minimizes the risk of side reactions that could impair foam stability. Furthermore, the polyol's viscosity molecular weight, and iodine value fall within the desirable range for rigid foam processing, promoting good flowability and PU structural integrity. These characteristics are consistent with literature-reported values and confirm the suitability of p-CDEA for RPUF formulations.[33–35]

Synthesis of C-doped SNP

To identify the chemical structures in the synthesized SNP, the FTIR spectra of the SNP samples with and without κ-carrageenan are analyzed and shown in Fig. 2A. Both showed the same peaks of typical SNP, such as the –OH stretch at 3415 cm^{-1}, Si–O–Si asymmetry shown at 1064 cm^{-1}, symmetric Si–O–Si peaks at 793 cm^{-1}, Si–O–Si bending vibration at 475 cm^{-1}, and a small peak at 1643 cm^{-1} for adsorbed water.[36,37]

Crystalline characteristics of the SNP are shown in Fig. 2B via the XRD spectra and summarized in Table 2. This agrees with the literature in which the crystalline structure of SNP is formed above or equal to 700 °C.[38] The major peaks of the spectra correspond to a cristobalite form of silica at Miller–Bravais indices of (101), (111), (102), and (200).[39] Using Scherrer's formula, the crystalline size at (101) of both SNPs was calculated to be 35.5 nm and 38.9 nm, respectively. Also, it can be observed that there is an increase in crystal volume with the addition of κ-carrageenan. This can be attributed to the straining of the crystal lattice. This strain resulted in the exposure of positive silicon atoms, leading to enhanced catalytic and improved dispersion due to the accessibility of active
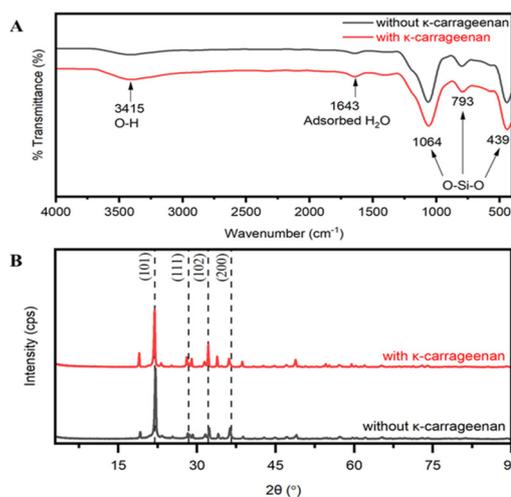
Table 1 Key properties of the produced p-CDEA used for rigid polyurethane foam synthesis

Properties	p-CDEA (this study)
Hydroxyl (OH) number, mg KOH per g	361 ± 12
Acid value, mg KOH per g	4.3 ± 1.3
Viscosity, mPa	696 ± 18
Molecular weight, Da	986 ± 25
Iodine value, g I$_2$ per 100 g	5.6 ± 1.5

Fig. 2 (A) Fourier transform infrared spectroscopy (FTIR) and (B) X-ray diffraction (XRD) spectra of synthesized silica nanoparticles (SNP) of both with and without κ-carrageenan.

Table 2 Summary data of crystallite size and crystallinity index of silica nanoparticles (SNP) with and without κ-carrageenan

Sample	Average crystallite size (nm)	Miller–Bravais indices (101) peak (Nm)	d-Spacing		Lattice parameters		Unit cell volume (Å³)	Crystallinity index (%)
			d_{100} (Å)	d_{002} (Å)	$a = b$ (Å)	c (Å)		
SNP without κ-carrageenan	35.53	35.3	4.02	3.12	4.95	6.88	168.58	92.81
SNP with κ-carrageenan	47.45	38.9	4.05	3.18	4.97	6.99	172.66	90.43

sites within its crystal structure.[40,41] Moreover, a slight shifting of the peaks to the right can be discerned from Fig. 2B, suggesting the occurrence of doping.

XPS analysis was employed further to examine the synthesis and doping of the SNP samples. Fig. 3A depicts the broad scan analysis showing the characteristic peaks of Si 2p, S 2p, C 1s, and O 1s, thus proving successful SNP synthesis. By comparing Fig. 3B and C, the deconvoluted peaks at the Si 2p regions indicate the presence of Si–C and Si–S doping on the SNP with κ-carrageenan (Fig. 3C), with the former having greater intensity than the latter. C-doping is preferred to S-doping due to the similarity of the electron configuration of carbon and silicon. C-doping of silica was well-known to improve surface modification and induce uniform size in composite particles, making it useful for the chemical stability and biocompatibility of the particles as well as wide applications such as catalysis, energy storage, and organic synthesis.[42]

Fig. 4A and B show the SEM image and EDX of the SNP with κ-carrageenan, respectively. The SEM image shows SNP's highly agglomerated and porous formation, which is similar to related literature.[43] The EDX also shows a high silica content with both carbon and sulfur. Although the SEM image cannot highlight the nanoscale size of the synthesized SNP, the particle size distribution shown in Fig. 4C and the crystalline size from XRD show that the size of SNP ranges around 30 nm.
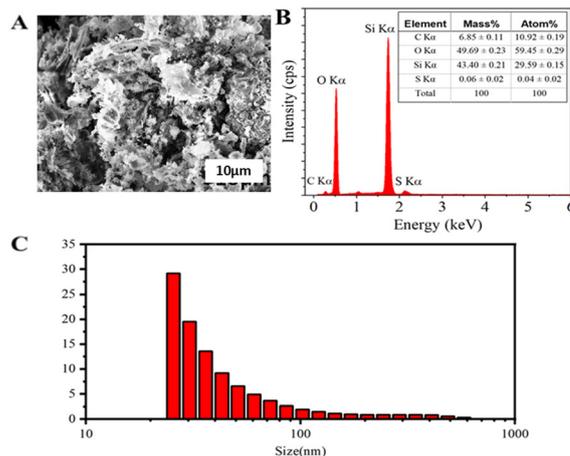
Fig. 4 (A) Scanning electron microscope (SEM), (B) energy dispersive X-ray (EDX), and (C) particle size distribution of silica nanoparticles (SNP) with κ-carrageenan.

Synthesis and characterization of SNP-RPUF

FTIR spectra of SNP-RPUF composite between 4000 and 400 cm^{-1} are shown in Fig. 5. Fig. 5A shows the prominent IR peaks of PUs, particularly at 3320 cm^{-1} and 1601 cm^{-1}, which correspond to the amine (N–H) stretching and bending vibrations. These peaks generally support the formation of urethane linkages. Furthermore, it is observed that the intensity of the transmittance of all bonds increases as the addition of SNP also increases until 0.3% and then decreases thereafter. This increase in intensity is associated with the densification of the RPUF matrix brought by the SNP acting as a nucleation site.[44] Surfaces of nanoparticles, such as silica, become the active site at which polymer structure undergoes reactive formation.[45] Concurrently, the decrease in intensity is due to the agglomeration of SNPs. The densification of the PU matrix due to SNP is mainly the hydrogen-bonding (H-bonding) of the hydroxyl groups of SNP to the ester, ether, and amide groups of the RPUF. As the SNP increases, the surface tension between the SNP decreases, which causes intermolecular H-bonding in its hydroxyl groups.[46]

In Fig. 5B, it can be observed that there are trends in the shifting of the peaks. These changes are attributed to the H-bonding between the SNP and the RPUF matrix. In Fig. 5C, D, E and F, in-depth peak shifting was observed at the peaks ~3320 cm^{-1}, ~1715 cm^{-1}, ~1200 cm^{-1}, and ~916 cm^{-1} are rep-
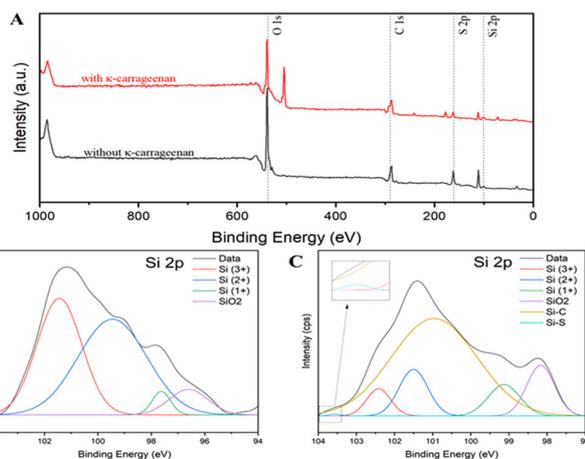
Fig. 3 (A) X-ray photoelectron spectroscopy (XPS) spectra of synthesized silica nanoparticles (SNP) of both with and without κ-carrageenan including the deconvolution of the Si 2p region of the XPS for (B) without κ-carrageenan and (C) with κ-carrageenan.
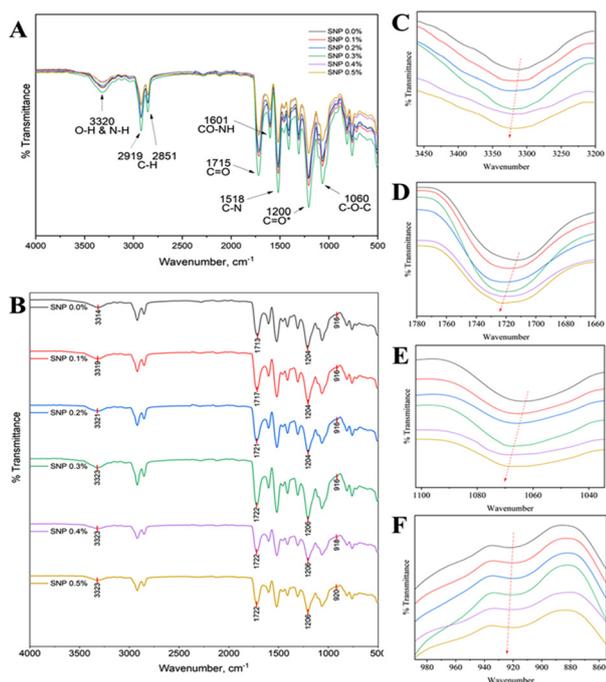
Fig. 5 Fourier transform infrared spectroscopy (FTIR) spectra of silica nanoparticles-rigid polyurethane foam (SNP-RPUF) (A and B) with focused regions on (C) amine (N–H), (D) carbonyl (C=O) of ester groups, (E) C=O of amide groups, and (F) silicon groups.

Fig. 6 Scanning electron microscope (SEM) micrographs (50× magnification) of rigid polyurethane foam (RPUF) foams at varying additions of silica nanoparticles (SNP).

resented by the amine (N–H stretching), ester (C=O), amide (C=O*), and silicon (Si) groups, respectively. The increase in peak shifts observed at the OH, NH, C=O, and C=O* groups until SNP 0.3% represents the SNP-RPUF matrix's H-bonding increase. Similarly, at the Si peaks, it can also be observed that the peak shifts increase after SNP 0.3%, which relates to the peak shifts with the other functional groups. The combined peak shifts show that with the addition of an SNP of up to 0.3%, H-bonding from the SNP to RPUF increases. After 0.3% addition of SNP, H-bonding between SNP molecules dominates over the H-bonding of the SNP-RPUF matrix due to saturation of added SNP.

The morphology of the SNP-RPUF samples is shown in the SEM in Fig. 6. The foam cells of the RPUF without the addition of SNP (SNP 0.00%) are more irregular and larger compared to the RPUF with SNP. This shows that SNP has a significant effect on the morphology of the foam. Table 3 summarizes the SEM and pycnometric analyses, including average cell size, closed cell content, and cell density. It is also apparent that average cell size, cell density, and closed cell content are optimal at 0.3% SNP loading. This supports the H-bonding of the SNP principle as it acts as a nucleating agent in the formation of the RPUF matrix. With more SNPs, there would be more polymer networks in the RPUF matrices than spaces representing the foam bubbles. A related study[47] stated that SNP leads to the growth of a larger number of cells with reduced cell size and uniform dispersion within the RPUF matrix.
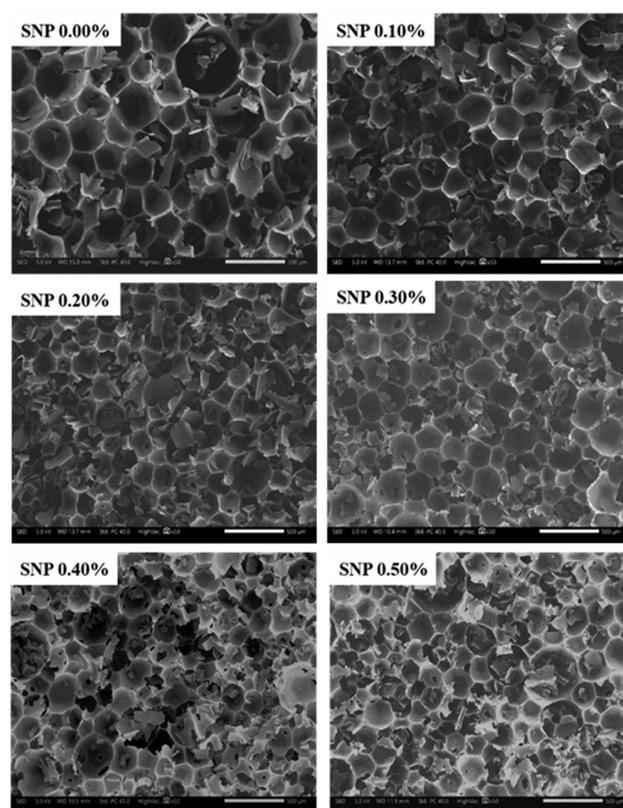
The mechanical properties of the SNP-RPUF samples are summarized in Fig. 7. In Fig. 7B, the compressive strength of RPUF increases from 0.66 MPa to 1.27 MPa from 0.00% to 0.30% loading of the SNP and then decreases to 0.90 MPa at 0.50% SNP. The same trend is also observed with the compressive modulus in Fig. 7C. The trend of the mechanical strength of the RPUF is similar to both the chemical and morphological observations, which further proves the densification process of the SNP-RPUF matrix. The observed enhancement in compressive strength is closely related to the increase in foam density (Table 3). Denser polyurethane foams generally exhibit a more compact and uniform cell structure, which enhances resistance to compressive deformation. This improved mechanical performance is attributed to a higher number of load-bearing cell walls per unit volume and reduced cell size, both of which contribute to a more robust foam network. Also, at 0.30% SNP, the increase in strength was about 92.42% compared to pure RPUF, which is higher than that of other studies.[48]

Compared to other studies, the mechanism involved in the high increase of strength is mainly due to the higher amount of amine moieties present in the bio-polyol. H-bonding of SNP to nitrogen-containing groups is stronger and more likely to bond than the other H-bonding predominantly present in RPUF. The other H-bonding for RPUF mainly includes oxygen from esters and ethers, which are single or double-bonded to

Table 3 Cell size, cell density, closed cell content, and apparent density of rigid polyurethane foam (RPUF) at varying addition of silica nanoparticles (SNP)
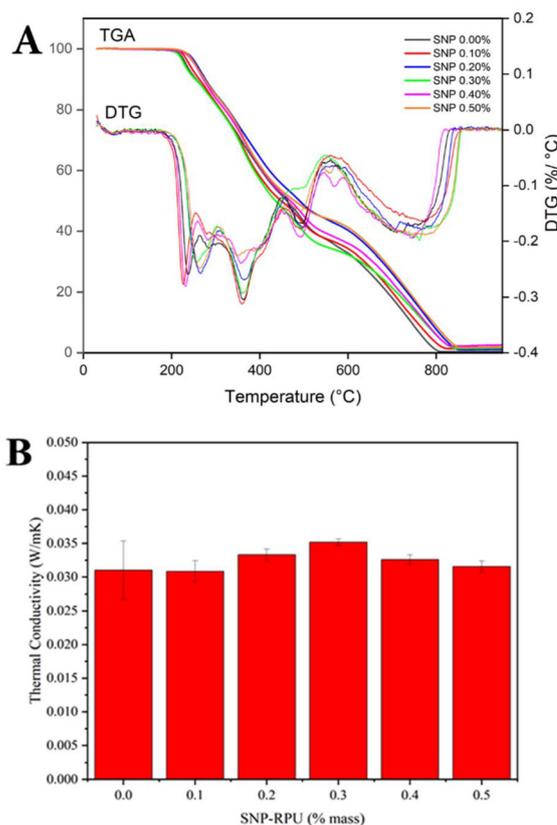
Sample	Cell size (μm)	Cell density (cells per μm^3)	Closed cell content (%)	Apparent density (kg m^{-3})
SNP 0.00%	245.98 ± 75.90	6.89 ± 0.59	69.23 ± 5.95	25 ± 1.5
SNP 0.10%	208.77 ± 56.75	14.08 ± 2.62	78.54 ± 4.74	27 ± 1.5
SNP 0.20%	200.79 ± 56.32	19.64 ± 1.26	85.35 ± 6.35	30 ± 1.5
SNP 0.30%	178.18 ± 42.14	25.78 ± 0.61	92.37 ± 2.19	32 ± 1.5
SNP 0.40%	191.87 ± 56.57	17.50 ± 0.65	77.94 ± 2.88	35 ± 1.6
SNP 0.50%	190.30 ± 40.64	15.13 ± 1.32	76.64 ± 6.71	37 ± 1.6
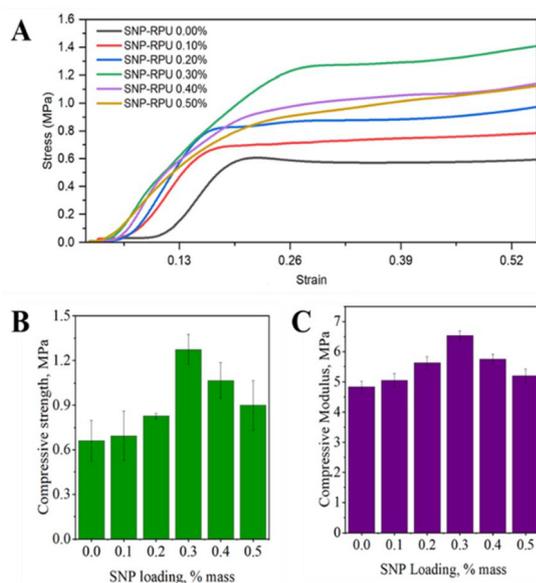
Fig. 7 Mechanical properties of rigid polyurethane foam (RPUF) with varying addition of silica nano-particles (SNP): (A) Compressive stress–strain curve, (B) compressive strength, and (C) compressive modulus.

Fig. 8 (A) Thermogravimetric analysis (TGA) and (B) thermal conductivity of rigid polyurethane foam (RPUF) at varying addition of silica nanoparticles (SNP).

carbon. This results in steric hindrances to the oxygen, mitigating its electronegativity and further reducing the strength and tendency to form H-bonds.[49] A possible contributing mechanism could be the cross-linking of SNP with the diethanoamine groups, as crosslinking typically improves the mechanical properties of RPUs.[48,50]

The mechanical strength of SNP-reinforced PU (SNP-RPUF) was further enhanced by introducing C-doping into the SNPs. C-doping generates crystal vacancies by substituting some of the silicon atoms with carbon atoms. Since the ionic sizes of silicon atoms are larger than carbon atoms, their replacement creates additional spaces, exposing unreplaced silicon atoms.[51,52] These exposed silicon atoms exhibit electrophilic properties, giving additional reactive sites and increasing the likelihood of (OH) groups coming from the bio-polyol to attach onto the surface of SNP. The increased presence of OH groups on the SNP surface enhances H-bonding and promotes polymer densification, leading to a significant increase in mechanical strength.

Fig. 8A shows the thermogravimetric analysis of the SNP-RPUF samples. RPUF showed multiple degradation stages

similar to related literature using coconut diethanolamine.[26] The analysis consists of up to four stages at around 250 °C, 360 °C, 500 °C, and 750 °C. The first stage comprises the soft or polyol segments, the second stage for the hard or isocyanate stage, and the other stages consist of residues such as amines, complex ethers, branched alcohols, and benzene alkyls.[52] Unlike the trend with the compressive strength, the highest amount of char was observed at 0.5% addition of SNP, with about 2.88% char with first-stage decomposition at 258 °C, compared to the 0.0% addition having 0.34% char with 232 °C first-stage decomposition temperature. This trend indicates that the synthesized RPUF has good thermal stability and could contribute to its flame retardancy.[53–56]

1362 | *RSC Appl. Polym.*, 2025, **3**, 1356–1365

© 2025 The Author(s). Published by the Royal Society of Chemistry

Fig. 8B shows the thermal conductivity of the SNP-RPUF samples. The thermal conductivity ranges between 0.030–0.035 W m^{-1} K^{-1}, with a trend to slightly increase as SNP is added up to 0.3% before it decreases. For RPUF, it is more beneficial to have lower density and larger cells to increase the amount of entrapped gas, which helps to reduce thermal transfer. Although the addition of the SNP reduces its insulation application, the thermal conductivity is still within range for commercial RPUF of 0.025–0.040 W m^{-1} K^{-1}.[57] Also, the high value of closed cell content further inhibits the increase of thermal conductivity of the SNP-RPUF as it reduces the diffusion of entrapped gas to the atmosphere, as the movement of gases adds convective thermal transfer.

Overall, this study significantly contributes to environmental remediation by advancing the use of bio-based RPUF reinforced with green SNP derived from RHA and carbon-doped using κ-carrageenan. Incorporating these sustainable nanomaterials enhances the mechanical, thermal, and structural properties of the RPUF, positioning it as a viable material for environmental remediation applications such as pollutant sequestration, waste management, and water purification. Utilizing RHA as a feedstock not only provides a sustainable, renewable source of silica but also addresses the environmental challenges associated with rice husk disposal. The improved properties of the SNP-reinforced RPUF, including enhanced thermal stability and mechanical strength, expand its potential for use in protective coatings, insulation, and structural components for environmental remediation systems. By replacing conventional, petrochemical-based foams with this bio-based alternative, this work supports the development of eco-friendly materials that reduce environmental pollution. Additionally, the study highlights the utility of green synthesis methods in producing nano-materials that align with the principles of sustainability, circular economy, and waste valorization, paving the way for integrating sustainable materials into industrial applications to mitigate environmental impacts.

Conclusion

This study aimed to synthesize a high-performance RPUF using C-doped SNP from RHA, κ-carrageenan, and amine-functionalized bio-polyol derived from coconut oil. The synthesized C-doped SNP's composition, crystallinity, and doping were confirmed *via* FTIR, XRD, DLS, SEM-EDX, and XPS analyses. The C-doping of SNP with κ-carrageenan resulted in lattice expansion within the crystal structure, enhancing the reactivity of Si2+ atoms with other materials. Mechanical test of the RPUF with varying addition of SNP indicated that optimal compressive strength was achieved at a 0.30% SNP addition, resulting in a 92.42% increase. Peak shifting of the FTIR results of the SNP-RPUF revealed that intermolecular H-bonding between the RPUF and SNP was the leading cause for the improved mechanical properties,

which is further proved by the increase in cell density and % closed cells from the SEM and pycnometric analyses. The thermogravimetric analysis demonstrated optimal thermal resistance to degradation at a 0.5% SNP addition, with thermal conductivity ranging from 0.030 to 0.035 W m^{-1} K^{-1}. This study successfully synthesized a highly bio-based RPUF with excellent strength and thermal stability and promising applications as insulation and structural support for roofs, pipes, and wall panels. The synthesized RPUF demonstrated superior mechanical properties to conventional RPUF while utilizing renewable, eco-friendly, and cost-effective feedstocks, positioning it as a potential alternative to widely used RPUF.

Author contributions

All authors have made substantial contributions to the conception, design, acquisition of data, analysis, and/or interpretation of data for the work; participated in drafting and/or revising the manuscript critically for important intellectual content; approved the final version to be submitted; and agreed to be accountable for all aspects of the work in ensuring that questions related to the accuracy or integrity of any part of the work are appropriately investigated and resolved.

Author contributions are as follows: Carlo Kurt F. Osorio: conceptualization, methodology, formal analysis, data curation, investigation, validation, visualization, writing – original draft, writing – review and editing. Christine Joy M. Omisol: conceptualization, data curation, visualization, writing – original draft, writing – review and editing. Dan Michael A. Asequial: conceptualization, methodology, investigation, data curation, writing – review and editing. Blessy Joy M. Aguinid: conceptualization, methodology, formal analysis, writing – review and editing. Daisy Jane D. Erjeno: conceptualization, methodology, formal analysis. Kassandra Jayza Gift D. Tejas: conceptualization, investigation, formal analysis. Roger G. Dingcong Jr.: conceptualization, methodology, writing – review and editing. Tomas Ralph B. Tomon: conceptualization, visualization, formal analysis. Renzo Miguel R. Hisona: conceptualization, visualization, formal analysis. Andrei E. Etom: formal analysis, data curation, investigation. Ann Pearl G. Triana: formal analysis, data curation, investigation. Gerard G. Dumancas: validation, resources, writing – review and editing. Arnold C. Alguno: validation, resources, funding acquisition. Joshua B. Zoleta: formal analysis, data curation, investigation. Roberto M. Malaluan: validation, resources, funding acquisition. Arnold A. Lubguban: conceptualization, methodology, validation, funding acquisition. All authors have read and approved the final manuscript.

Conflicts of interest

There are no conflicts to declare.

Data availability

All data necessary to reproduce the findings of this study are contained within the main article. Additional raw data not fully described herein are available from the corresponding author upon reasonable request.

Acknowledgements

References

1 V.-C. Niculescu, *Front. Mater.*, 2020, **7**, 36.

2 H. Li, B. Cheng, W. Gao, C. Feng, C. Huang, Y. Liu, P. Lu and H. Zhao, *Nanotechnol. Rev.*, 2022, **11**, 2928–2964.

3 P. S. Shinde, P. S. Suryawanshi, K. K. Patil, V. M. Belekar, S. A. Sankpal, S. D. Delekar and S. A. Jadhav, *J. Compos. Sci.*, 2021, **5**, 75.

4 P. Singh, S. Srivastava and S. K. Singh, *ACS Biomater. Sci. Eng.*, 2019, **5**, 4882–4898.

5 C. Zhuang and Y. Chen, *Nanotechnol. Rev.*, 2019, **8**, 562–572.

6 A. Nyabadza, É. McCarthy, M. Makhesana, S. Heidarinassab, A. Plouze, M. Vazquez and D. Brabazon, *Adv. Colloid Interface Sci.*, 2023, **321**, 103010.

7 A. Saha, P. Mishra, G. Biswas and S. Bhakta, *RSC Adv.*, 2024, **14**, 11197–11216.

8 J. Sarkar, D. Mridha, J. Sarkar, J. T. Orasugh, B. Gangopadhyay, D. Chattopadhyay, T. Roychowdhury and K. Acharya, *Biocatal. Agric. Biotechnol.*, 2021, **37**, 102175.

9 P. U. Nzereogu, A. D. Omah, F. I. Ezema, E. I. Iwuoha and A. C. Nwanya, *Hybrid Adv.*, 2023, **4**, 100111.

10 O. Bounekta, R. Doufnoune, A. Ourari, F. Riahi and N. Haddaoui, *J. Fundam. Appl. Sci.*, 2019, **11**(1), 200–226.

11 P. G. Jeelani, P. Mulay, R. Venkat and C. Ramalingam, *Silicon*, 2020, **12**, 1337–1354.

12 S. Sharada and S. A. Rehaman, *YMER Digit.*, 2022, **21**, 309–405.

13 C. Y. Rahimzadeh, A. A. Barzinjy, A. S. Mohammed and S. M. Hamad, *PLoS One*, 2022, **17**, e0268184.

14 Polyurethanes Market by Raw Material Type, Product, End User – Global Forecast 2025–2030.

15 Southeast Asia Polyurethane Market Size, Share & COVID-19 Impact Analysis, By Product Type (Rigid Foam, Flexible Foam, Molded Foam, Elastomers, Adhesives & Sealants, Coatings, and Others), By Application (Furniture, Construction, Electronics, Automotive & Transportation, Packaging, Footwear, and Others), and Regional Forecast, 2022–2029.

16 H. Sardon, D. Mecerreyes, A. Basterretxea, L. Avérous and C. Jehanno, *ACS Sustainable Chem. Eng.*, 2021, **9**, 10664–10677.

17 L. N. A. Hipulan, R. G. Dingcong, D. J. E. Estrada, G. G. Dumancas, J. C. S. Bondaug, A. C. Alguno, H. P. Bacosa, R. M. Malaluan and A. A. Lubguban, *ACS Omega*, 2024, 13112–13124.

18 Global Biofoam Market Market Size Likely to Grow at a CAGR of 22.1% By 2034.

19 A. Agrawal, R. Kaur and R. S. Walia, *e-Polym.*, 2019, **19**, 411–420.

20 M. Kumar and R. Kaur, *e-Polym.*, 2017, **17**, 517–521.

21 K. Skleničková, S. Abbrent, M. Halecký, V. Kočí and H. Beneš, *Crit. Rev. Environ. Sci. Technol.*, 2022, **52**, 157–202.

22 A. Agrawal, R. Kaur and R. S. Walia, *Eur. Polym. J.*, 2017, **95**, 255–274.

23 D. Cho and J. K. Oh, *Nanomaterials*, 2023, **13**, 2035.

24 A. B. Francés and M. V. N. Bañón, *IOP Conf. Ser.: Mater. Sci. Eng.*, 2014, **64**, 012020.

25 M. M. A. Nikje and Z. M. Tehrani, *Des. Monomers Polym.*, 2011, **14**, 263–272.

26 R. G. Dingcong, R. M. Malaluan, A. C. Alguno, D. J. E. Estrada, A. A. Lubguban, E. P. Resurreccion, G. G. Dumancas, H. H. Al-Moameri and A. A. Lubguban, *RSC Adv.*, 2023, **13**, 1985–1994.

27 U. Kalapathy, A. Proctor and J. Shultz, *Bioresour. Technol.*, 2002, **85**, 285–289.

28 C. A. Maharani, E. Budiasih and S. Wonorahardjo, *IOP Conf. Ser.: Mater. Sci. Eng.*, 2019, **546**, 042021.

29 J. C. S. Bondaug, R. G. Dingcong, L. N. Hipulan, P. C. Ochigue, G. G. Dumancas, A. C. Alguno, R. M. Malaluan, A. A. Lubguban and H. P. Bacosa, *ACS Appl. Polym. Mater.*, 2024, **6**, 6875–6887.

30 A. Ivdre, A. Abolins, I. Sevastyanova, M. Kirpluks, U. Cabulis and R. Merijs-Meri, *Polymers*, 2020, **12**, 738.

31 R. G. Dingcong, M. A. N. Ahalajal, L. C. C. Mendija, R. J. G. Ruda-Bayor, F. P. Maravillas, A. I. Cavero, E. J. C. Cea, K. J. M. Pantaleon, K. J. G. D. Tejas, E. A. Limbaga, G. G. Dumancas, R. M. Malaluan and A. A. Lubguban, *ACS Omega*, 2024, 13100–13111.

32 R. Zhang, J. Chen, Y. Zhu, J. Zhang, G. Luo, P. Cao, Q. Shen and L. Zhang, *Polymers*, 2020, **12**, 315.

33 R. G. Dingcong, D. B. Radjac, F. L. A. M. Alfeche, A. C. O. Dizon, K. J. G. D. Tejas, R. M. Malaluan, H. H. Al-Moameri, G. G. Dumancas, A. C. Alguno and A. A. Lubguban, *Sustainability*, 2023, **15**, 12082.

34 L. C. C. Mendija, R. G. Dingcong, F. L. A. M. Alfeche, H. H. Al-Moameri, G. G. Dumancas, N. P. B. Tan, R. M. Malaluan, A. C. Alguno and A. A. Lubguban, *Sustainability*, 2024, **16**, 4587.

35 F. L. A. M. Alfeche, R. G. Dingcong, L. C. C. Mendija, H. H. Al-Moameri, G. G. Dumancas, A. A. Lubguban,

R. M. Malaluan, A. A. Alguno and A. A. Lubguban, *Sustainability*, 2023, **15**, 7148.

36 H. Helmiyati and R. P. Suci, *AIP Conf. Proc.*, 2019, **2168**, 1–7.

37 R. Ellerbrock, M. Stein and J. Schaller, *Sci. Rep.*, 2022, **12**, 11708.

38 M. J. Kaleli, P. K. Kamweru, J. M. Gichumbi and F. G. Ndiritu, *J. Chem. Eng. Mater. Sci.*, 2020, **11**, 24–30.

39 L. Ma, Y. Wang, Y. Wang and S. Fu, *Colloids Surf., A*, 2019, **580**, 123700.

40 G. Collins, K. Rahme, J. O'Connell and J. D. Holmes, *Catal. Sci. Technol.*, 2016, **6**, 7212–7219.

41 E. Moretto, C. Yan, R. Dieden, P. Steiner, B. Duez, D. Lenoble and J.-S. Thomann, *Polymers*, 2022, **14**, 1676.

42 T. Wu, Q. Ke, M. Lu, P. Pan, Y. Zhou, Z. Gu, G. Cui and H. Lu, *Catalysts*, 2022, **12**, 573.

43 S. Sankar, S. K. Sharma, N. Kaur, B. Lee, D. Y. Kim, S. Lee and H. Jung, *Ceram. Int.*, 2016, **42**, 4875–4885.

44 P. C. D. Ochigue, R. G. Dingcong, J. C. S. Bondaug, B. C. G. Magalong, G. G. Dumancas, C. S. Gutierrez, A. C. Alguno, R. M. Malaluan, A. A. Lubguban and H. P. Bacosa, *Sustainability*, 2024, **16**, 8540.

45 B. Merillas, F. Villafañe and M. Á. Rodríguez-Pérez, *Polymers*, 2021, **13**, 2952.

46 E. Burgaz and C. Kendirlioglu, *Polym. Test.*, 2019, **77**, 105930.

47 S. A. Bonab, J. Moghaddas and M. Rezaei, *Polymer*, 2019, **172**, 27–40.

48 K.-M. Li, J.-G. Jiang, S.-C. Tian, X.-J. Chen and F. Yan, *J. Phys. Chem. C*, 2014, **118**, 2454–2462.

49 J. K. Saha, M. M. Rahman, M. B. Haq, D. A. Al Shehri and J. Jang, *Polymers*, 2022, **14**, 1701.

50 P. J. Trzebiatowska, A. S. Echart, T. C. Correas, A. Eceiza and J. Datta, *Prog. Org. Coat.*, 2018, **115**, 41–48.

51 E. N. Sgourou, D. Timerkaeva, C. A. Londos, D. Aliprantis, A. Chroneos, D. Caliste and P. Pochet, *J. Appl. Phys.*, 2013, **113**, 113506.

52 P. Guo, B. Wang, M. Bauchy and G. Sant, *Cryst. Growth Des.*, 2016, **16**, 3124–3132.

53 R. Kaur and M. Kumar, *Mater. Res. Express*, 2020, **7**, 015333.

54 A. Agrawal, R. Kaur and R. S. Walia, *J. Appl. Polym. Sci.*, 2019, **136**, 48250.

55 A. Agrawal, R. Kaur and R. S. Walia, *Fire Mater.*, 2019, **43**, 917–927.

56 A. Agrawal and R. Kaur, *Integr. Ferroelectr.*, 2019, **202**, 20–28.

57 B. Hadała, B. Zygmunt-Kowalska, M. Kuźnia, A. Szajding and T. Telejko, *Thermochim. Acta*, 2024, **731**, 179659.